




Synthesis and spectral investigation of colorimetric receptors for the dual detection of copper and acetate ions: application in molecular logic gates

Srikala Pangannaya, Arshiya Kaur, Makesh Mohan, Keyur Raval, Dillip Kumar Chand & Darshak R. Trivedi

To cite this article: Srikala Pangannaya, Arshiya Kaur, Makesh Mohan, Keyur Raval, Dillip Kumar Chand & Darshak R. Trivedi (2017) Synthesis and spectral investigation of colorimetric receptors for the dual detection of copper and acetate ions: application in molecular logic gates, *Supramolecular Chemistry*, 29:8, 561-574, DOI: [10.1080/10610278.2017.1298764](https://doi.org/10.1080/10610278.2017.1298764)

To link to this article: <http://dx.doi.org/10.1080/10610278.2017.1298764>

 View supplementary material 

 Published online: 23 Mar 2017.

 Submit your article to this journal 

 View related articles 

 View Crossmark data 



Synthesis and spectral investigation of colorimetric receptors for the dual detection of copper and acetate ions: application in molecular logic gates

Srikala Pangannaya^a, Arshiya Kaur^b, Makesh Mohan^c, Keyur Raval^d, Dillip Kumar Chand^b and Darshak R. Trivedi^a

^aSupramolecular Chemistry Laboratory, National Institute of Technology Karnataka (NITK), Surathkal, India; ^bDepartment of Chemistry, Indian Institute of Technology Madras (IITM), Chennai, India; ^cDepartment of Physics, National Institute of Technology Karnataka (NITK), Surathkal, India; ^dDepartment of Chemical Engineering, National Institute of Technology Karnataka (NITK), Surathkal, India

ABSTRACT

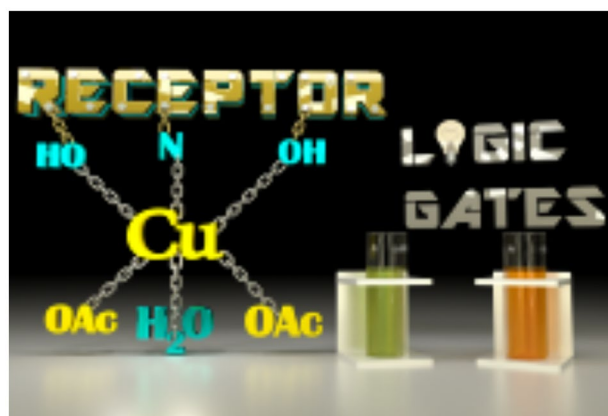
Colorimetric receptors **L1**, **L2** and **L3** possessing –OH functionality as binding site and –NO₂ as signalling unit with varied positional substitution of –OMe functionality has been designed and synthesised by simple Schiff base condensation reaction. Receptors **L1**, **L2** and **L3** showed selective response towards AcO[−] ion among other interfering monovalent anions viz., F[−], Cl[−], Br[−], I[−], NO₃[−], HSO₄[−] and H₂PO₄[−]. **L2** imparts high selectivity towards AcO[−] ion assisted by push-pull effect of –NO₂ and –OMe functionality in conjugation with imine linkage. The binding constant for L2–OAc complex was found to be $9.04 \times 10^4 \text{ M}^{-2}$. **L2** exhibited a detection limit of 0.61 ppm towards NaOAc. The selectivity of **L1** towards Cu²⁺ ions with a lower detection limit of 1.81 ppm implies the role of electron donating –OMe in favouring the coordinative interaction of hetero atoms of **L1** with Cu²⁺ ions. The selective detection of AcO[−] and Cu²⁺ ions is further established with OR and INHIBIT logic gate application of receptors **L1**, **L2** and **L3** correspondingly. The colorimetric studies reveal the role of OMe functionality in the selective detection of AcO[−] and Cu²⁺ ions in aqueous media.

ARTICLE HISTORY

Received 20 October 2016
Accepted 19 February 2017

KEYWORDS

Schiff base; substitution effect; colorimetric; dual sensor; logic gate




1. Introduction

Supramolecular chemistry of host–guest interaction is a vibrant area of research owing to its applicability in biochemistry and environmental science (1). The design and synthesis of new artificial receptors have seen progressive path unveiling their utility in the detection of physiologically important anions and cations (2). Acetate ion has been one of the intriguing targets due to its significance in metabolic processes. The rate of acetate production and

sedimentation has been an indicator of organic decomposition in marine sediments. Moreover, utility of acetate ion is realised in the manufacture of paper, plastics, dyes and paints (3). Correspondingly, past few years have witnessed a number of receptors for the detection of biologically and environmentally relevant transition metal cations. Copper being the third most abundant essential trace element is required in optimum amount for regulation

CONTACT Darshak R. Trivedi  darshaktrivedi@nitk.ac.in

 Supplemental data for this paper is available online at <http://dx.doi.org/10.1080/10610278.2017.1298764>

of fundamental physiological process (4). Copper ion is known to promote bone development, cellular respiration, nerve function regulation and haemoglobin synthesis (5).

Numerous technologies such as atomic absorption spectroscopy, X-ray photoelectron spectroscopy, voltammetry, inductively coupled plasma emission or mass spectrometry have been developed for the detection of trace amount of cations and anions (6). In reality, sophisticated instrumentation, time factor and cost are the reasons that strictly limit the usage of these techniques on the real time basis (7). Thus far, numerous colorimetric receptors have been developed by researchers by virtue of the detection of anions and cations at ease without resorting to sophisticated instrumentation (8–14). In this direction, numerous reports are available in the literature wherein researchers have developed artificial receptors which exhibit excellent anion binding property both in solution and solid states (15–21). Simple urea-based cleft-type receptors have been designed and synthesised by researchers involving structural manipulation of receptors appended to a signalling unit which drives selective detection of anions (22). Most of the receptors reported so far for the detection of acetate ions exhibit interference from fluoride and phosphate ions (23–25). Selective detection of anions has been one of the thrust area of research in anion receptor chemistry and development of new design strategies involving effective binding sites and signalling unit is gaining prime importance.

In the last few decades, the colorimetric detection of anions and cations based on molecular devices has been a subject of extensive research interest (26). The integration of molecular logic gates into working automation and arithmetic systems has revealed the clear idea of a molecular scale calculator (27–29). Molecular logic gates involve chemical inputs (30) and generate output signals (31) that operate in a wireless mode. This highlights the advantages and potential of logic gate devices in computation on a nanometre scale over the silicon-based devices eventually leading to the possibility to load an array of Boolean functions onto a single molecule.

In this regard, finding the utility of both Cu^{2+} and AcO^- ions, we report three new isomeric receptors with varied positional substitution of $-\text{OMe}$ functionality following binding site-signalling unit approach dedicated to bind both anions and cations. Furthermore, the dual ion sensing property could be an impetus to study molecular logic gate applications.

2. Experimental section

2.1. Materials and methods

All the chemicals used in the present study were procured from Sigma-Aldrich, Alfa Aesar or Spectrochem and were

used as received without further purification. All the solvents were purchased from SD Fine, India, were of HPLC grade and used without further distillation.

Melting point was measured on Stuart SMP3 melting-point apparatus in open capillaries. Infrared spectra were recorded on Bruker FTIR spectrometer. UV/Vis spectroscopy was performed with Thermo Scientific Genysys 10S spectrophotometer in standard 3.0 mL quartz cell with 1 cm path length. The ^1H NMR spectra were recorded on Bruker Ascend (400 MHz) instrument using TMS as internal reference and $\text{DMSO}-d_6$ as solvent. Resonance multiplicities are described as s (singlet), d (doublet), t (triplet) and m (multiplet).

2.2. Synthesis of L1

To 197.44 mg (1.29 mmol) of the 2-hydroxy-5-methoxybenzaldehyde, 200 mg (1.29 mmol) of 2-amino-5-nitrophenol was added. To this mixture, approximately 10 mL of methanol and a drop of glacial acetic acid (catalyst) were added and the reaction mixture was sonicated at room temperature for 5 min. The beaker was covered with aluminium foil with pinholes for slow evaporation of solvent. The solid product was recrystallised in methanol in 75% yield. Melting point: 192 °C

^1H NMR ($\text{DMSO}-d_6$, 400 MHz, ppm): δ 12.35 (OH, s), 10.25 (OH, s), 8.98 (HC=N, s), 7.79–7.77 (Ar CH, d), 7.49–7.29 (Ar CH, s), 6.94–6.91 (Ar CH, d), 6.62–6.61 (Ar CH, d), 6.20 (Ar CH, s), 3.76 (OMe, s). ^{13}C NMR ($\text{DMSO}-d_6$, 100 MHz, ppm): 56.05, 109.10, 111.43, 115.42, 118.5, 119.8, 121.02, 121.95, 142.92, 146.16, 151.57, 152.34, 155.24, 164.72. FT-IR (cm^{-1}): 3372 (OH), 2998 (Ar C-H), 1607 (CH=N), 1506 (aromatic C=C), 1231 (C–O, stretching). Mass: calculated: 288.07, obtained: 289.08 (M + H) $^+$.

2.3. Synthesis of L2

To 197.44 mg (1.29 mmol) of the 2-hydroxy-4-methoxybenzaldehyde, 200 mg (1.29 mmol) of 2-amino-5-nitrophenol was added. To this mixture approximately 10 mL of methanol and a drop of glacial acetic acid (catalyst) were added and the reaction mixture was sonicated at room temperature for 5 min. The beaker was covered with aluminium foil with pinholes for slow evaporation of solvent. The solid product was recrystallised in methanol in 75% yield. Melting point: 195 °C

^1H NMR ($\text{DMSO}-d_6$, 400 MHz, ppm): δ 13.78 (OH, s), 10.73 (OH, s), 8.94 (HC=N, s), 7.79 (Ar CH, s), 7.77 (Ar CH, s), 7.56 (Ar CH, s), 7.53 (Ar CH, s), 6.56 (Ar CH, s), 6.47 (Ar CH, s), 6.46 (Ar CH, s), 3.82 (OMe, m). ^{13}C NMR ($\text{DMSO}-d_6$, 100 MHz, ppm): 56.03, 101.45, 107.82, 111.13, 113.56, 115.70, 120.30, 134.91, 141.81, 145.78, 151.20, 163.45, 165.06, 165.53. FT-IR (cm^{-1}): 3389 (OH), 3082 (Ar C-H), 1585 (CH=N), 1521

(aromatic C = C), 1205 (C–O, stretching). Mass: calculated: 288.07, obtained: 289.08 (M + H)⁺.

2.4. Synthesis of L3

To 197.44 mg (1.29 mmol) of the 2-hydroxy-3-methoxybenzaldehyde, 200 mg (1.29 mmol) of 2-amino-5-nitrophenol was added. To this mixture approximately 10 mL of methanol and a drop of glacial acetic acid (catalyst) was added and the reaction mixture was sonicated at room temperature for 5 min. The beaker was covered with aluminium foil with pinholes for slow evaporation of solvent. The solid product was recrystallised in methanol in 75% yield. Melting point: 198 °C

¹H NMR (DMSO-*d*₆, 400 MHz, ppm): δ 13.26 (OH, s), 10.76 (OH, s), 9.03 (HC=N, s), 7.8–7.6 (Ar CH, d), 7.57 (Ar CH, s), 7.17–6.94 (Ar CH, s), 6.92 (Ar CH, s), 6.90 (Ar CH, s), 3.83 (OMe, m). ¹³C NMR (DMSO-*d*₆, 100 MHz, ppm): 56.37, 111.23, 115.57, 116.48, 119.02, 119.70, 120.97, 120.97, 124.41, 142.12, 146.33, 148.61, 151.93, 151.54, 165.30. FT-IR (cm⁻¹): 3438 (OH), 2830 (Ar C–H), 1631 (CH=N), 1528 (aromatic C=C), 1256 (C–O, stretching). Mass: calculated: 288.07, obtained: 289.08 (M + H)⁺.

3. Results and discussion

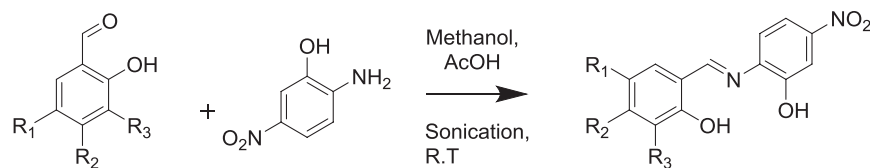
Receptors **L1**, **L2** and **L3** have been synthesised in good yield by simple Schiff base condensation reaction of methoxy substituted salicylaldehyde with 2-amino,5-nitrophenol using acetic acid as catalyst and methanol as solvent (Scheme 1). TLC has been performed to confirm the product formation and the receptors **L1**, **L2** and **L3** have been characterised by standard spectroscopic techniques

such as FT-IR and ¹H-NMR in order to confirm the structural aspects.

3.1. UV-vis spectrophotometric studies

Receptors **L1**, **L2** and **L3** by virtue of varied positional substitution of –OMe functionality at *para*, *meta* and *ortho* position to the –OH substitution is expected to exhibit significant colorimetric response in the presence of anions. The presence of –NO₂ group as signalling unit is known to produce a colour change visible to the naked eye in the anion binding process.

The anion binding properties of receptors **L1**, **L2** and **L3** were investigated by UV-vis spectroscopic studies. In the colorimetric analysis, 1 equiv. of 10⁻² M solution of tetrabutylammonium (TBA) salts of anions such as F⁻, Cl⁻, Br⁻, I⁻, NO₃⁻, HSO₄⁻, H₂PO₄⁻ and AcO⁻ (10⁻² M DMSO) were added to 2 mL of 10⁻⁴ M solutions of **L1**, **L2** and **L3** in acetonitrile. In the visual investigation, the pale yellow solution of receptor **L1** turned deep orange on addition of 1 equiv. of AcO⁻. Receptor **L2** and **L3** exhibited colour change from yellow to deep red and bright pink on addition of 1 equiv. of AcO⁻ ion. Mild colour change was observed with the addition of F⁻ ions indicating weak interaction of F⁻ with receptors **L1**, **L2** and **L3**. In contrast, no obvious colour changes were observed upon addition of other anions. In order to confirm the observed colour changes, UV-vis spectra has been recorded with the addition of 1 eq. of anions to 2 ml of ACN solution of receptors **L1**, **L2** and **L3**. The colour change is represented in Figures 1–3. The unbound receptor **L1** and **L2** displayed absorption maxima centred at ~ 381 nm whereas **L3** exhibited two absorption bands at 304 nm and 367 nm. The higher energy band at 304 nm



Receptor	R ₁	R ₂	R ₃
L1	OMe	H	H
L2	H	OMe	H
L3	H	H	OMe

Scheme 1. Synthesis of L1, L2 and L3.

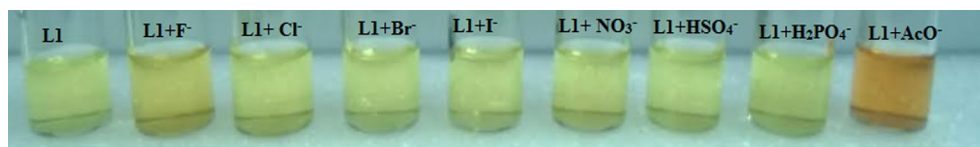


Figure 1. Colour change of **L1** in ACN (10^{-4} M) before and after addition of 1 equiv. of anions.

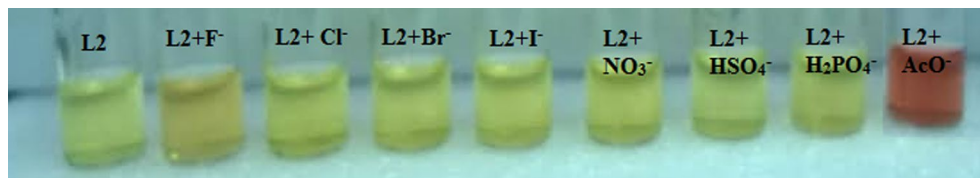


Figure 2. Colour change of **L2** in ACN (10^{-4} M) before and after addition of 1 equiv. of anions.

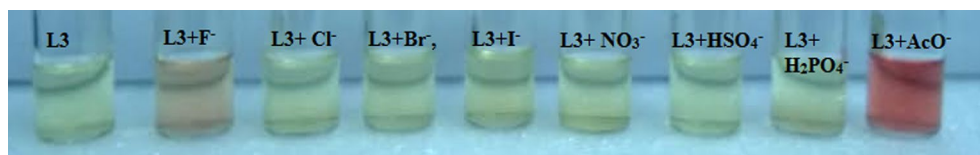


Figure 3. Colour change of **L3** in ACN (10^{-4} M) before and after addition of 1 equiv. of anions.

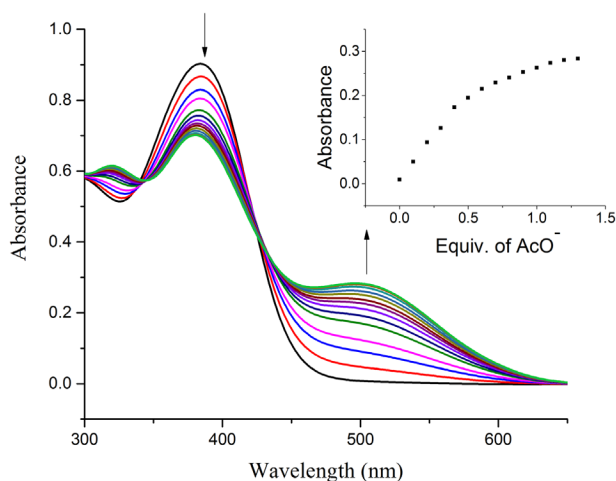


Figure 4. UV-vis absorption spectra of **L1** in ACN (10^{-4} M) upon titration with tetrabutylammonium acetate (10^{-2} M in DMSO). Note: Inset plot represents the binding isotherm at 496 nm.

corresponds to the π - π^* transitions of azomethine group and lower energy band at 381 nm and 367 nm in **L2** and **L3** represent the overall intramolecular charge transfer transitions within the receptor molecule.⁽³²⁾ Appearance of red shift band upon addition of 1 eq. of AcO^- ion to receptors **L1**, **L2** and **L3** at 496 nm, 518 nm and 520 nm correspondingly indicate the formation of receptor-anion complex. The UV-vis spectra are represented in Figure S7, S8 and S9 (Supporting information).

To gain further insight into the anion binding interaction with the receptor, UV-vis spectrophotometric titration studies has been performed. On successive addition of 0.1 eq. of TBAOAc (10^{-2} M in DMSO) to receptor **L1** (10^{-4} M in ACN), the band at 381 nm decreased in its intensity with the appearance of a new band at 496 nm as shown in Figure 4. The red shift observed corresponds to the bifurcated hydrogen bond interaction of AcO^- ion with the two OH groups present on the receptor. Yet, the position of OMe being para to one of the OH moiety indicates the weaker acidity of -OH proton and relative stronger bond existing between oxygen and hydrogen. The possibility of intramolecular hydrogen bonding of second -OH functionality with imine nitrogen is relatively weaker as evidenced in the $^1\text{H-NMR}$ of unbound receptor **L1**. The tendency of OH proton to bind AcO^- ion is further enhanced owing to the greater basicity of the anion. Two isosbestic points at 425 and 340 nm were observed during the titration, indicating that the presence of two reacting species in the anion binding process. Benesi Hildebrand (B-H) plot indicates the 1:1 complexation for **L1**-acetate complex as indicated in Figure S10 (Supporting information). The binding ratio could be correlated to the ability of AcO^- ion to bind and deprotonate the one of OH functionality forming CH_3COOH by counteracting the intramolecular hydrogen bonding interactions within the receptor. The possibility of CH_3COOH to abstract proton from second -OH functionality generates ionic species $[\text{CH}_3\text{COOH}_2]^+$.

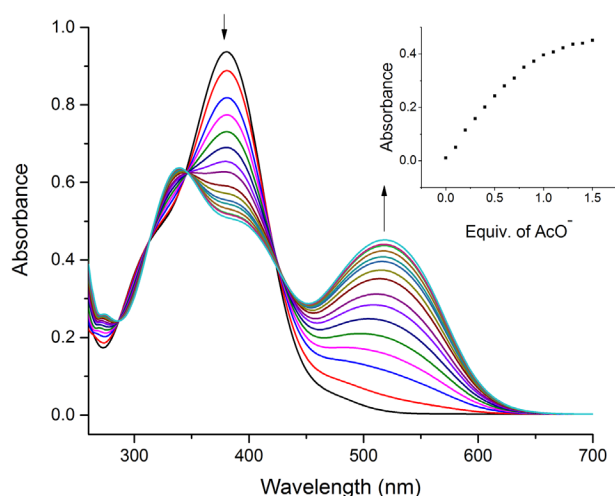


Figure 5. UV-vis absorption spectra of **L2** in ACN (10^{-4} M) upon titration with tetrabutylammonium acetate (10^{-2} M in DMSO). Note: Inset plot represents the binding isotherm at 518 nm.

The above mechanism could be an evidence for the hydrogen bonding ability of both –OH functionality.

Receptor **L2** (10^{-4} M in ACN) showed remarkable colorimetric response with the incremental addition of 0.1 eq. of AcO^- ion. Successive decrease in the original band centred at 381 nm with the growth of new red shift band at 518 nm is indicative of the strong anion-receptor interaction as shown in Figure 5. The presence of electron donating –OMe functionality para to the imine linkage, allows the –OH functionality to involve in intramolecular hydrogen bond interaction. The presence of intramolecular hydrogen bond is confirmed from the ^1H NMR spectrum which exhibits signal for –OH proton at δ 13.78 ppm (downfield). The presence of electron withdrawing – NO_2 functionality imparts the formation of strong intramolecular hydrogen bond of –OH of nitrophenyl group with the imine functionality. The conformational change of the receptor **L2** in the presence of AcO^- ions is more preferred in the anion binding followed by deprotonation of receptor **L2**. The preorganisation of receptor allows bifurcated hydrogen bond interaction between AcO^- and two OH functionalities of **L2**.

The stoichiometry of **L2**- AcO^- complex was determined by B–H plot. The linear plot obtained with the first power and second power of concentration of AcO^- ion clearly revealed the existence of at least two species of complexes (1:1 and 1:2 for **L2**: AcO^-). (33) (Figure S11 and S12 (Supporting information)). This could be the probable reason for the appearance of four isobestic points in the titration spectra. Binding ratio indicates the formation of dimer, $[(\text{CH}_3\text{COO})\text{H}_2]^+$ and $[\text{L2}]^{2-}$. The presence of four isobestic points observed at 424, 345, 314 and 286 nm indicates the presence of complex equilibrium process in the formation of **L2**- AcO^- ion complex.

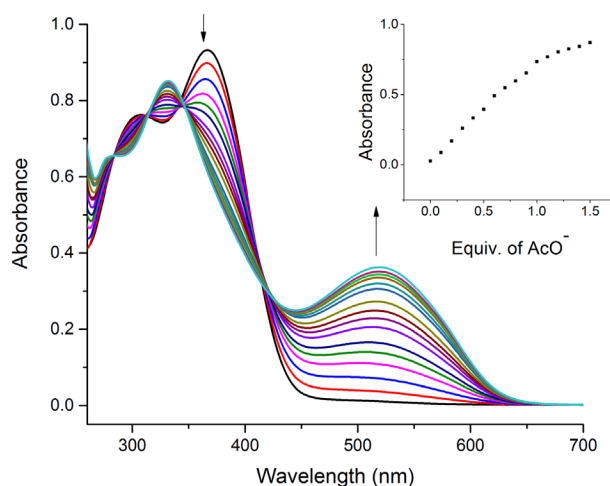


Figure 6. UV-vis absorption spectra of **L3** in ACN (10^{-4} M) upon titration with tetrabutylammonium acetate (10^{-2} M in DMSO). Note: Inset plot represents the binding isotherm at 520 nm.

UV-vis spectra of Receptor **L3** exhibited significant colorimetric response with the incremental addition of 0.1 eq of AcO^- ion. Unlike **L1** and **L2**, the receptor **L3** exhibited a varied colour change with a decrease in the bands centred at 304 and 367 nm with the emergence of new red shift band at 520 nm and a blue shift band at 350 nm as shown in Figure 6. The presence of –OMe at *meta* position relative to the imine linkage and at *ortho* position to the OH functionality of salicylaldimine represents a unique intramolecular hydrogen bond preferences of the –OH functionalities. The competitive nature of OMe and imine nitrogen to involve in hydrogen bond interaction with the OH functionality leads to downfield shift of –OH proton to δ 13.26 ppm. The relative decrease in the downfield shift of OH proton of **L3** in comparison with **L2** indicates relative weak nature of intramolecular hydrogen bond interaction facilitating strong binding of anions. As a consequence, NO_2 functionality imparts strong influence on the OH linked to imine functionality leading to deprotonation of receptor with CH_3COOH and $[\text{L3}]^-$ as end products. Thus formed CH_3COOH can further abstract another proton from hydroxyl functionality generating $[\text{CH}_3\text{COOH}_2]^+$ and $[\text{L3}]^{2-}$ as final products. Four isobestic points are observed at 415, 343, 313 and 284 nm indicating the involvement of interacting species in a complex equilibrium process (33) The B–H plot indicates the coexistence of two species with 1:1 and 1:2 binding ratio of **L3**- AcO^- ion complex as represented in Figure S13 and S14 (Supporting information).

Anion recognition has overwhelming applications in the medical, environmental, biological and industrial arenas which typically require aqueous media in order to mimic the physiological conditions. The design of selective anion receptors that function in aqueous solution has been a key challenge to supramolecular chemists. In this

regard, we have aimed to check the binding ability of **L1**, **L2** and **L3** towards sodium salt of AcO^- ion in aqueous media. It was observed that addition of 1 equiv. of 10^{-2} M solution of NaOAc (10^{-2} M in H_2O) changed the pale yellow colour of the receptor **L1** to orange as represented in Figure 7. **L2** exhibited significant colour change in the presence of 1 equiv. of 10^{-2} M solution of NaOAc (10^{-2} M in H_2O) from pale yellow to red as shown in Figure 8. **L3** displayed a colour change from pale yellow to bright pink implying the efficiency of the receptor in combating the solvent interferences as given in Figure 9.

The titration of **L1** with incremental addition of 0.1 eq. of NaOAc resulted in red shift of the original absorption band to 490 nm with isobestic point at 429 nm as seen in Figure S15(Supporting information). B–H plot revealed the 1:1 binding ratio of **L1**- AcO^- complex as shown in Figure S16 (Supporting information). Titration studies performed with incremental addition of 0.1 eq. of NaOAc to **L2** indicated red shift of the band to 512 nm with isobestic points at 426, 346, 313 and 284 nm as given in Figure S17(Supporting information). B–H plot indicated the formation of 1:1 and 1:2 complex in the binding process as represented in Figure S18 and S19 (Supporting information). Titration studies with the successive addition of AcO^- ion to solution of **L3** indicated shift in absorption band to 519 nm with isobestic points at 415, 343, 314 and 271 nm reflective of the complex formation. Titration profile is shown in Figure S20 (Supporting information). B–H plot indicated the formation of 1:1 and 1:2 complex as shown in Figure S21 and S22 (Supporting information). **L1**, **L2** and **L3** could be considered as synthetic anion receptor that can operate effectively in water, surpassing solvent interferences.

The presence of hetero atoms in the receptors **L1**, **L2** and **L3** has been the driving force to check the cation sensing ability. Upon addition of 1 eq. of nitrate salt of cations (Na^+ , K^+ , Ca^{2+} , Mg^{2+} , Al^{3+} , Co^{2+} , Ni^{2+} , Cu^{2+} , Zn^{2+} , Cd^{2+} , Hg^{2+} and Pb^{2+}) to **L1**, **L2** and **L3**, significant colour change was observed in the presence of Cu^{2+} ion. The colour change is shown in Figure S23, S24 and S25 (Supporting information). In naked-eye inspection, the receptor **L1** turns from pale yellow to pale orange on addition of 1 eq. of Cu^{2+} ion. **L2** and **L3** exhibited a colour change from pale yellow to orange-yellow on addition of 1 eq. of Cu^{2+} ion. In contrast, no significant changes were witnessed upon addition of other cations. In order to confirm the observed colour changes, UV–vis spectra have been recorded with the addition of 1 eq. of cations to 2 ml of ACN solution of receptors **L1**, **L2** and **L3**. The UV–vis spectra are represented in Figures 10–12.

The photophysical properties of **L1**, **L2** and **L3** have been studied to confirm the binding process. The red shift of band to 490, 477 and 467 nm indicates complexation

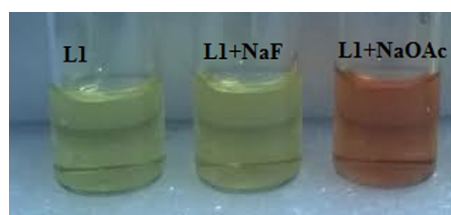


Figure 7. Colour change of **L1** in acetonitrile (10^{-4} M) before and after addition of 1 equiv. of NaF and NaOAc.

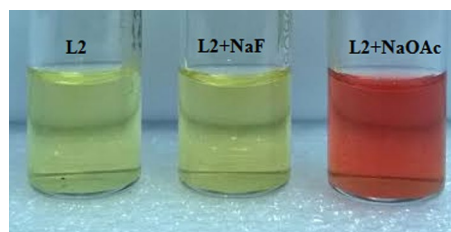


Figure 8. Colour change of **L2** in acetonitrile (10^{-4} M) before and after addition of 1 equiv. of NaF and NaOAc.

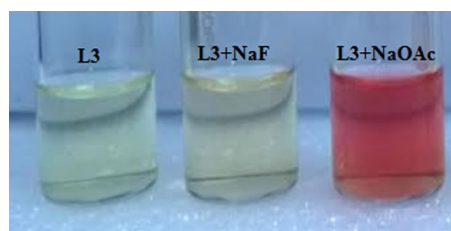


Figure 9. Colour change of **L3** in acetonitrile (10^{-4} M) before and after addition of 1 equiv. of NaF and NaOAc.

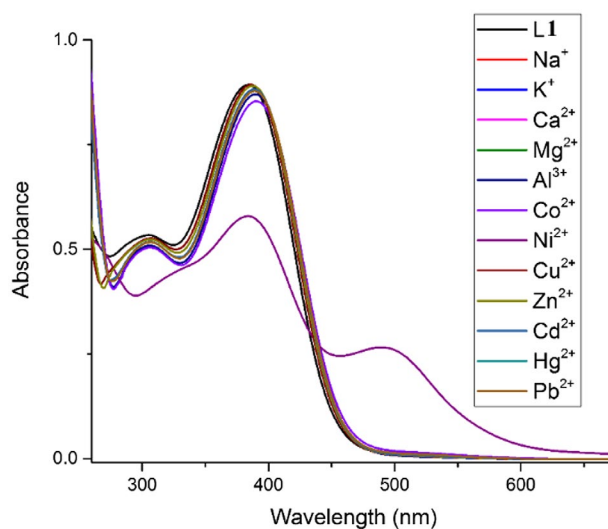


Figure 10. UV–vis absorption spectra of **L1** in ACN (10^{-4} M) upon addition of 1 equiv. of nitrate salts of a variety of cations.

of receptor with Cu^{2+} ion in 1:1, 1:1 and 1:1 binding ratio, respectively. Titration profile of **L1**, **L2** and **L3** with incremental addition of Cu^{2+} ion is shown in Figure S26, S28 and S30 (Supporting information). The corresponding

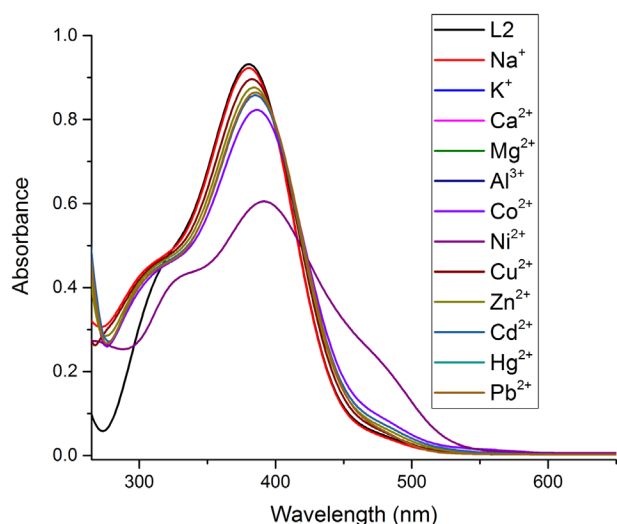


Figure 11. UV-vis absorption spectra of **L2** in ACN (10^{-4} M) upon addition of 1 equiv. of nitrate salts of a variety of cations.

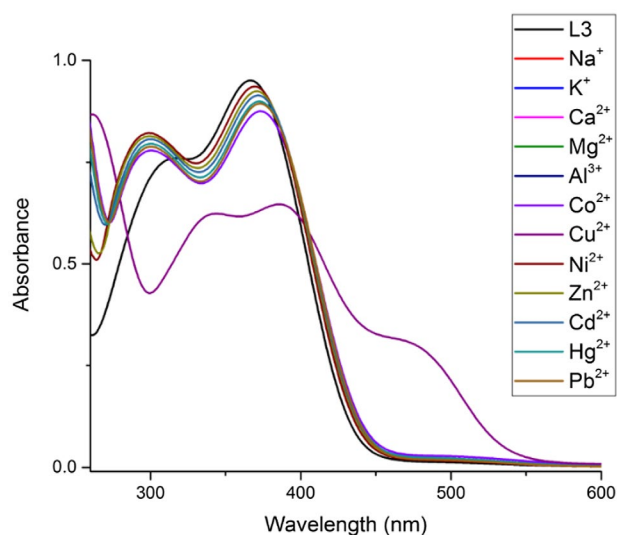


Figure 12. UV-vis absorption spectra of **L3** in ACN (10^{-4} M) upon addition of 1 equiv. of nitrate salts of a variety of cations.

B-H plot is shown in Figure S27, S29 and S31 (Supporting information).

Mechanistically, maximum red shift in **L1** can be attributed to the change in structural conformation of receptor on interaction with Cu^{2+} indicating the coordinative interaction between the lone π pair of the donor hetero-atoms OH and imine nitrogen which are conjugated to the π system of the receptor and the cation. Consequently, there is an increase in conjugation of the receptor in a tightly bound complex with Cu^{2+} , resulting in planarisation of complex and red-shift (34). However, no such considerable change was induced by the addition of other metal ions.

The dual responsive nature of receptors **L1**, **L2** and **L3** towards AcO^- ion and Cu^{2+} ion throws light on the ability of

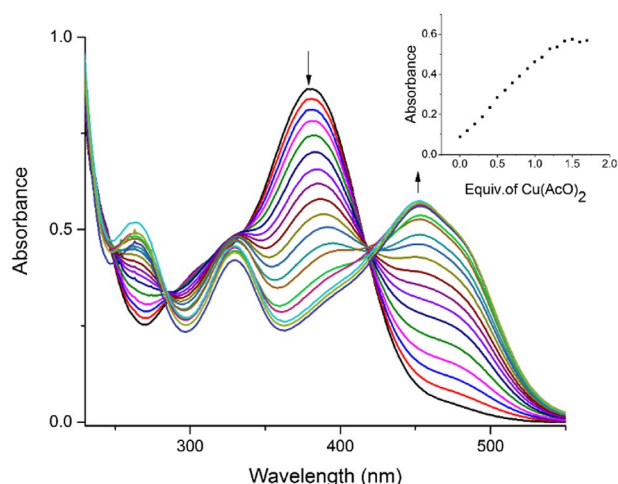


Figure 13. UV-vis absorption spectra of **L2** in ACN (10^{-4} M) upon titration with $\text{Cu}(\text{OAc})_2$ in H_2O (10^{-2} M). Inset plot represents binding isotherm at 453 nm.

the receptor to bind metal acetates, in particular $\text{Cu}(\text{OAc})_2$. With an aim to envisage the simultaneous sensing of AcO^- and Cu^{2+} ion, UV-vis titration studies has been performed with the incremental addition of $\text{Cu}(\text{OAc})_2$ to receptors **L1**, **L2** and **L3**. The addition of $\text{Cu}(\text{OAc})_2$ to 10^{-4} M DMSO solution of **L1**, **L2** and **L3** resulted in visual colour change from pale yellow to pale red, yellow and deep yellow, respectively, as shown in Figure S32 (Supporting information).

Receptor **L1** exhibited a red shift of original absorption band to 502 nm which is approximately closer to the titrimetric response observed for TBAOAc and $\text{Cu}(\text{NO}_3)_2$ individually. The binding of $\text{Cu}(\text{OAc})_2$ by **L1** was confirmed by the presence of clear isosbestic points at 340 and 421 nm as seen in Figure S33 (Supporting information). Receptor **L2** produced a new red shift band at 453 nm with the gradual disappearance of band at 380 nm at the expense of new blue shift band at 330 nm indicative of diminishing intramolecular hydrogen bonding interactions within the receptor. This is shown in Figure 13. The red shift band is in good agreement with the titrimetric response observed with $\text{Cu}(\text{NO}_3)_2$ alone nullifying the role of AcO^- ion in the binding process. The absence of well-defined isosbestic points indicates the presence of significant side reactions. Titration of $\text{Cu}(\text{OAc})_2$ with receptor **L3** revealed a new red shift band at 466 nm, being similar to the bare $\text{Cu}(\text{NO}_3)_2$ implies the strong binding of Cu^{2+} ion. The appearance of clear isosbestic points at 281, 318, 340 and 405 nm signifies the complex equilibrium process involved in the binding process as presented in Figure 14. B-H plot of **L1**, **L2** and **L3** with $\text{Cu}(\text{OAc})_2$ exhibited stoichiometric ratio of 1:1 as represented in Figure S34, S35 (Supporting information) and Figure 15 and the proposed binding mechanism is shown in Scheme 2.

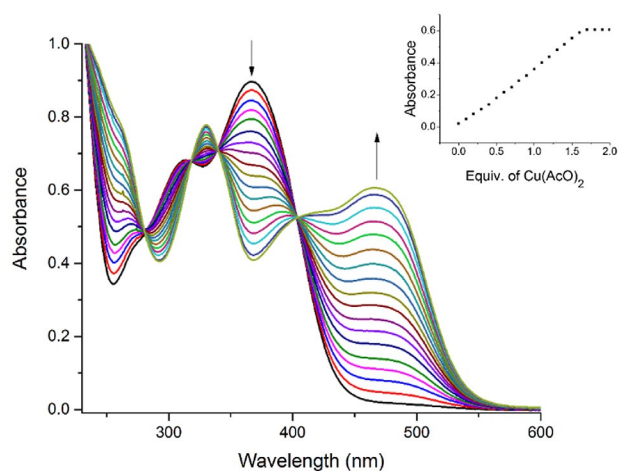


Figure 14. UV-vis absorption spectra of **L3** in ACN (10^{-4} M) upon titration with $\text{Cu}(\text{OAc})_2$ in H_2O (10^{-2} M). Inset plot represents binding isotherm at 466 nm.

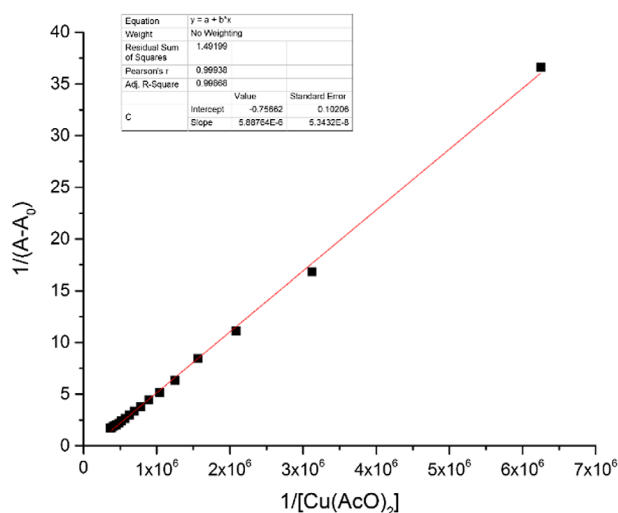
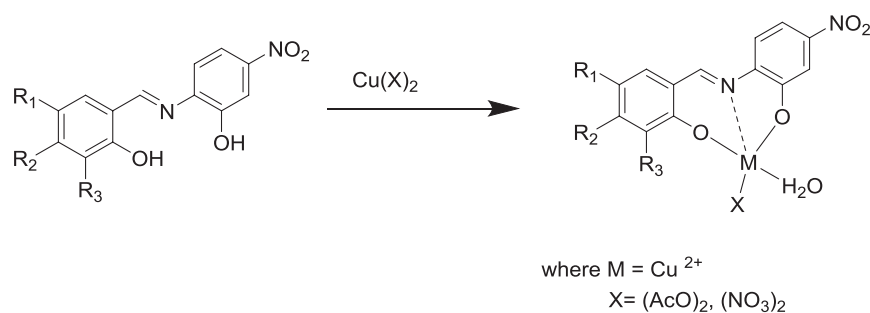


Figure 15. B-H plot for 1:1 **L3**- $\text{Cu}(\text{OAc})_2$ complex.



Scheme 2. Proposed binding mechanism of **L1**, **L2** and **L3** with $\text{Cu}(\text{OAc})_2$ and $\text{Cu}(\text{NO}_3)_2$.

Table 1. Binding constant and detection for **L1**, **L2** and **L3** in the presence of TBAOAc, NaOAc and Cu^{2+} ions.

Ions	Binding constant (10^2)			Detection limit (ppm)		
	L1 (M^{-1})	L2 (M^{-2}) ^a and (M^{-1}) ^b	L3 (M^{-2}) ^a and (M^{-1}) ^b	L1	L2	L3
TBAOAc	4.07	336.93 ^a 3.36 ^b	208.88 ^a 2.08 ^b	3.76	5.27	4.5
NaOAc	4.82	904.08 ^a 9.04 ^b	300.92 ^a 3.00 ^b	0.82	0.61	0.82
Cu^{2+}	1.55	1.29	0.86	1.8	3.28	4.6

^a1:2 receptor-acetate complex.

^b1:1 receptor-acetate complex.

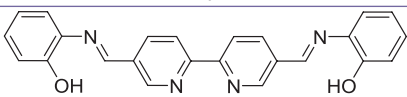
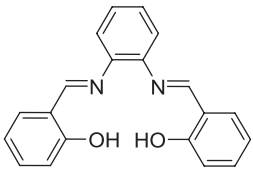
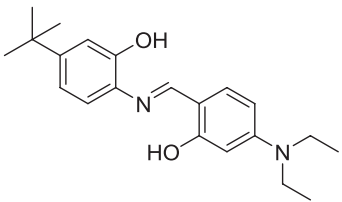
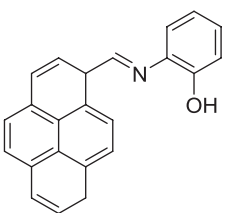
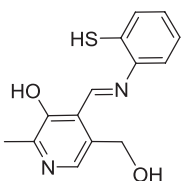
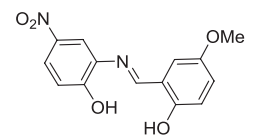
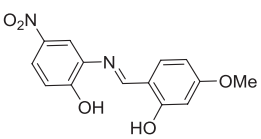
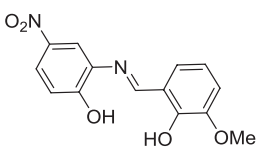
The binding constant has been calculated using B-H equation (35) and the values are tabulated in Table 1. Lower detection limit (LOD) of 0.61 ppm towards AcO^- ion has been achieved with **L2** indicating its practical utility. LOD of 1.8 ppm with Cu^{2+} reflects the role of **L1** as a colorimetric receptor in practical applications. The lower detection limit of **L2** towards NaAcO in comparison with TBAOAc could be correlated with the nature of counter cation in the stabilising the negative charge on the receptor. TBA ion having larger size in comparison with Na^+ ion renders meagre influence on stabilising the deprotonated

receptor. Further, a comparison of the present sensors with the previously reported ones has been tabulated in Table 2.

3.2. ¹H-NMR titration studies

With a view to unveil the nature of reaction between receptors **L1**, **L2** and **L3** with AcO^- ion, ¹H-NMR titration studies have been performed. With the incremental addition of 0.5, 1.0 eq. of TBAOAc to receptors **L1**, **L2** and **L3** the disappearance of both OH protons was observed indicating the formation of strong hydrogen bond interaction

Table 2. Data of comparison (medium, detection limit and binding constant) with other reported receptors.

Sl. No.	Receptor	Analytes	Binding constant (M^{-1})	Detection limit (M)	Medium	Ref.
1		$Cu(OAc)_2$	7.38×10^3	0.19×10^{-6}	DMSO	36
2		Cu^{2+}	$3.69 \times 10^6 (\pm 0.00208)$	Not reported	CH_3CN	37
3		Cu^{2+}	1.56×10^4	1.15×10^{-6}	CH_3CN/H_2O (9:1, v/v)	34
4		Cu^{2+}	1.96×10^6	9.72×10^{-7}	CH_3CN	38
5		AcO^-	3.12×10^4	Not reported	DMSO/DMSO/ H_2O (88:12, v/v).	39
6		Cu^{2+} OAc	1.55 4.82	2.8×10^{-5} 2.9×10^{-5}	ACN CH_3CN/H_2O (9:1, v/v)	This work
		Cu^{2+} (OAc)	1.29 904.08	9.6×10^{-6} 1.17×10^{-4}	ACN CH_3CN/H_2O (9:1, v/v)	
		Cu^{2+} (OAc)	0.86 300.92	7.2×10^{-5} 2.9×10^{-5}	ACN CH_3CN/H_2O (9:1, v/v)	

between AcO^- and receptor (34, 40). The aromatic proton signals underwent an upfield shift indicating the presence of through-bond effect which tends to increase the electron density on the aromatic ring. Correspondingly, **L1**, **L2** and **L3** exhibited a distinct downfield shift for imine proton from δ 8.96, 8.94, 9.04 to 9.3 ppm, representing the through-space interactions which polarise the C–H bonds in proximity of OH– AcO^- complex (41). The titration profile for **L1**, **L2** and **L3** is provided in Figures 16–18. The binding

mechanism has been proposed based on the above considerations and represented in Scheme 3.

The various possibilities involved in the intramolecular hydrogen bond interactions (42) in **L1**, **L2** and **L3** is provided in Scheme S4 (Supporting information). The binding mechanism has been proposed based on the UV–vis titration and 1H -NMR titration studies. **L1** exhibits hydrogen bonding interaction with AcO^- ion through –OH functionalities followed by single step deprotonation process

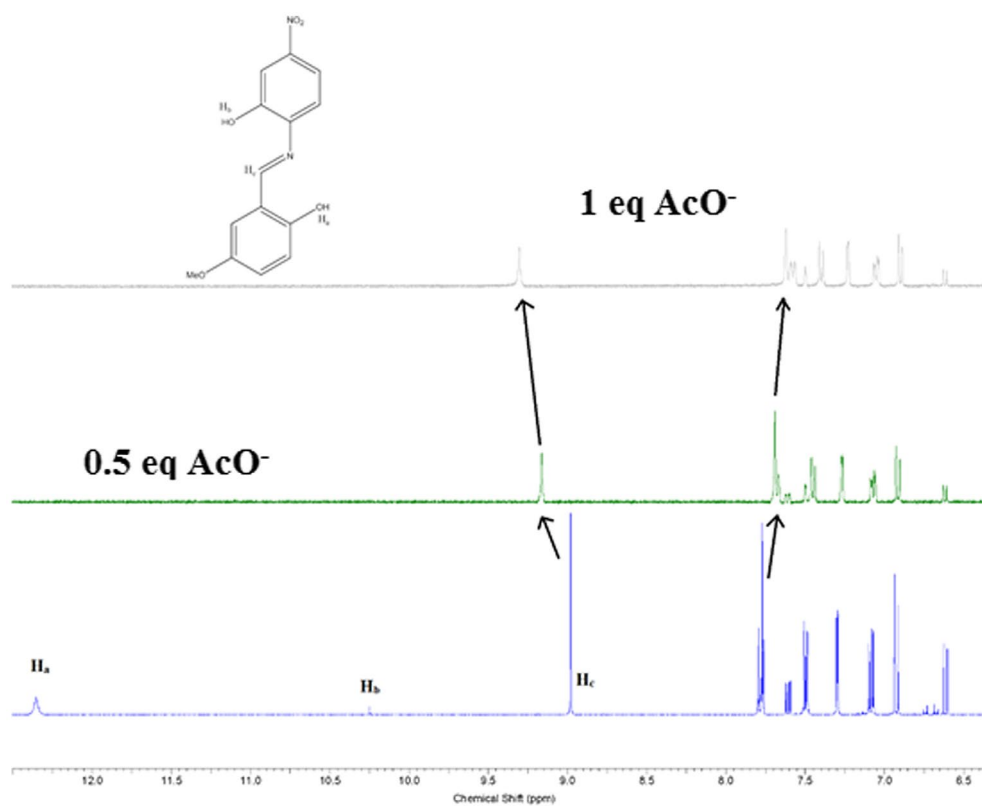


Figure 16. $^1\text{H-NMR}$ titration spectra of L1 with incremental addition of TBAOAc.

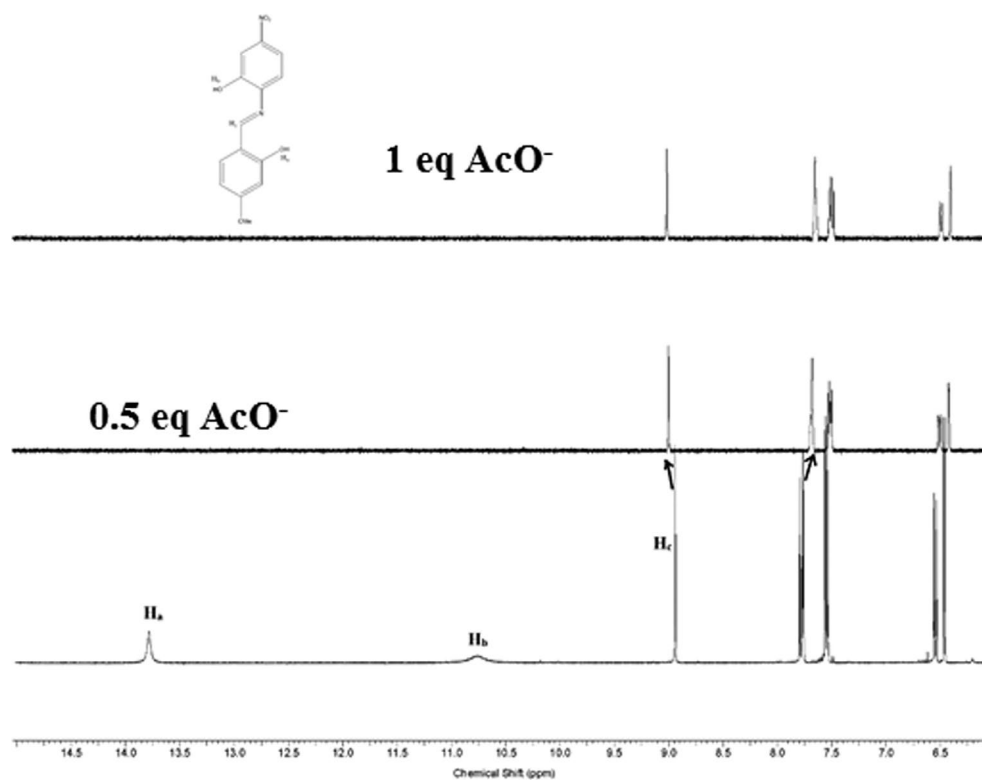


Figure 17. $^1\text{H-NMR}$ titration spectra of L2 with incremental addition of TBAOAc.

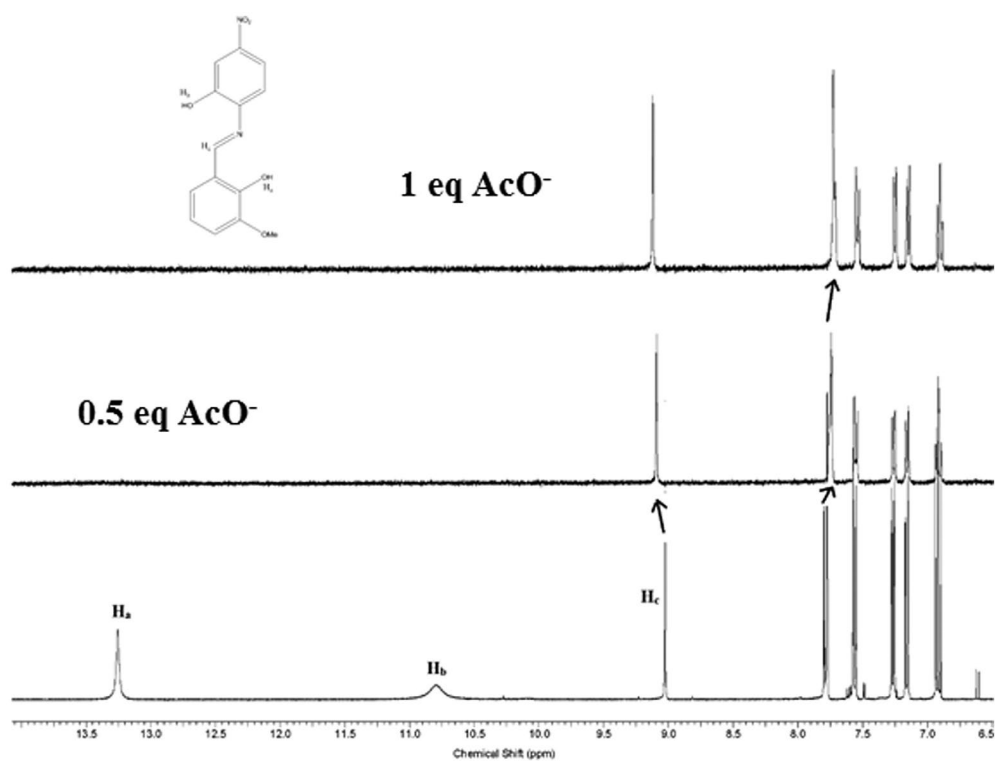
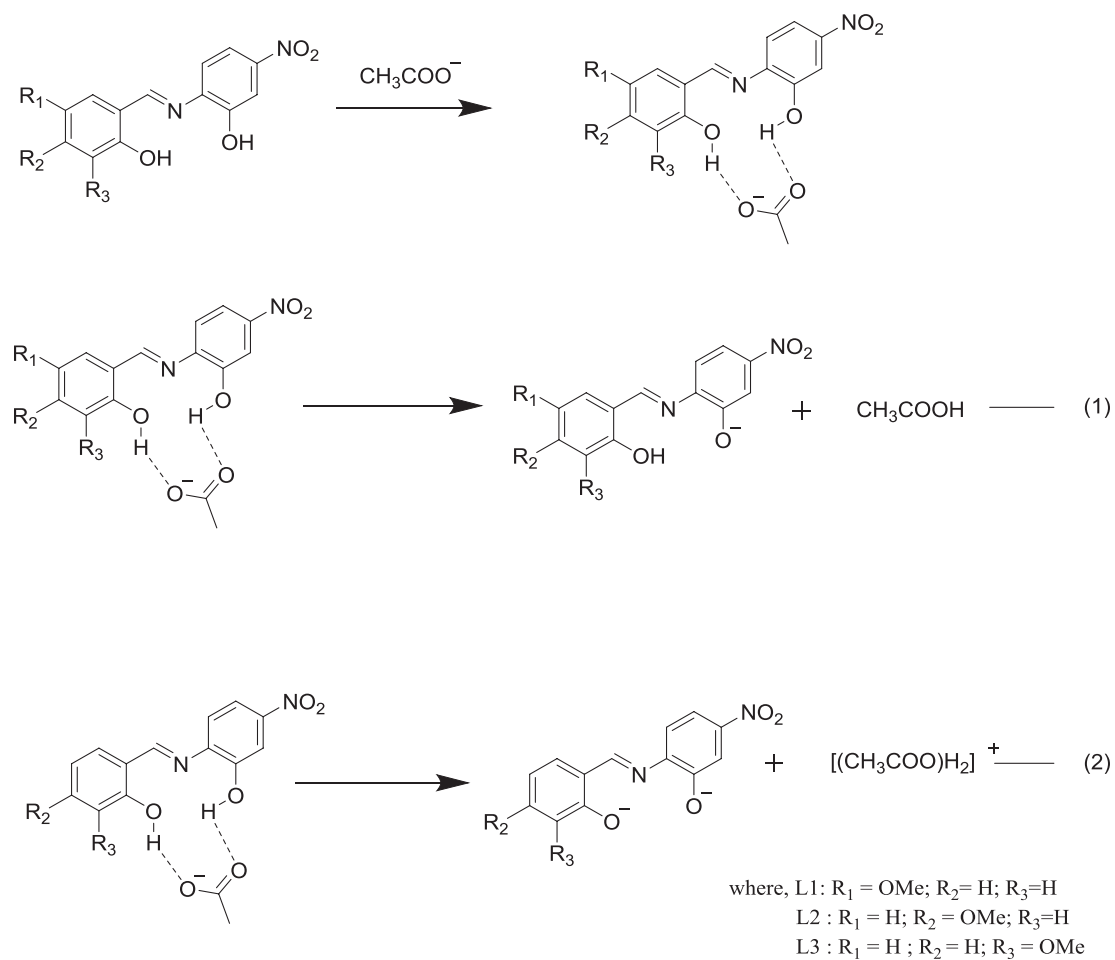


Figure 18. $^1\text{H-NMR}$ titration spectra of L3 with incremental addition of TBAOAc.



Scheme 3. Proposed binding mechanism of receptors L1, L2 and L3 with AcO^- ion.

Table 3. Truth table of Cu^{2+} and AcO^- ionic interaction with the **L1**.

Input	Input	Output
Cu^{2+}	AcO^-	496 nm
0	0	0
0	1	1
1	0	1
1	1	1

**Figure 19.** Representation of OR logic gate for receptor **L1**.

forming CH_3COOH . **L2** and **L3** undergo two step deprotonation process yielding $[(\text{CH}_3\text{COO})_2\text{H}_2]^+$ species confirming the binding ratio of 1:2 for **L2** / **L3**: AcO^- ion complex.

3.3. Logic gate applications

There is substantial interest in emerging molecular systems that imitates the behaviour of digital logic gates (43–46). The introduction of different inputs and their rule as logic gates is represented in the form of truth table. Receptor **L1**, **L2** and **L3** was explored for the design and construction of Boolean logic gates by the introduction of Cu^{2+} and AcO^- ionic inputs. These inputs and the corresponding optical outputs were coded with binary digits (01), which represents the 'on' and 'off' states. The ionic inputs for Cu^{2+} and AcO^- in the truth table were regarded as '0' when they are absent and '1' if they are present. Receptor **L1** exhibited a system response as that of a two input OR gate, while that of **L2** and **L3** exhibited an INHIBIT logic gate response.

Absorbance value at 496 nm regarded as the output signal upon the action of the Cu^{2+} and AcO^- ionic input. Receptor **L1** mimics the function of an OR gate which is one of the basic logic gates that implement logical disjunction. The truth table of Cu^{2+} and AcO^- ionic interaction with the **L1** clearly demonstrate the OR logical behaviour as given in Table 3. It is seen that the output of this molecular gate shoots to logic high state 1, if any of the input is 1. (Figure 19)

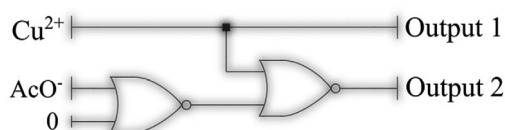
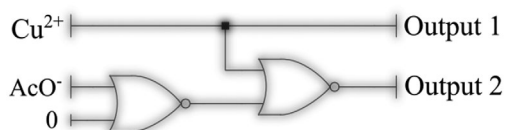
The inhibit gate consisting of integration of two NOR gate is important because of its non-commutative behaviour wherein the output signal is inhibited by one powerful input. In the present study, Cu^{2+} mainly decides the state of the signal output. Realisation of INHIBIT logical behaviour of receptor **L2** and **L3** for Cu^{2+} and AcO^- ions is as given in the truth table (Tables 4 and 5). The circuit is realised with two 2 input NOR gate wherein one of the input of NOR gate is set to 0 as shown in the circuit diagram Figures 20 and 21. **L2** and **L3** take in two inputs and exhibits two different

Table 4. Truth table of Cu^{2+} and AcO^- ionic interaction with the **L2**.

Input	Input	Output	Output
Cu^{2+}	AcO^-	477 nm	518 nm
0	0	0	0
0	1	0	1
1	0	1	0
1	1	1	0

Table 5. Truth table of Cu^{2+} and AcO^- ionic interaction with the **L3**.

Input	Input	Output	Output
Cu^{2+}	AcO^-	467 nm	520 nm
0	0	0	0
0	1	0	1
1	0	1	0
1	1	1	0

**Figure 20.** Representation of INHIBIT logic gate for receptor **L2**.**Figure 21.** Representation of INHIBIT logic gate for receptor **L3**.

response of absorbance at 477 and 518 nm. It is clear from the truth table that output 2 gives a value 1 upon binding of AcO^- ion alone. INHIBIT response of the gate could be realised with addition of $\text{Cu}(\text{OAc})_2$ ion to receptor **L2** and **L3**. The observed output value of 1 corresponds to the wavelength shift of receptor **L2** and **L3** to 477 and 467 nm found in the presence of $\text{Cu}(\text{NO}_3)_2$. The output value 0 signifies the absence of AcO^- ion in the signalling process.

Conclusions

In conclusion, we have presented a series of simple colorimetric receptors **L1**, **L2** and **L3** synthesised by Schiff base condensation reaction and characterised by standard spectroscopic techniques. UV-vis and $^1\text{H-NMR}$ titration studies confirm the hydrogen bond interaction between phenolic proton and acetate ion which is mirrored in the higher binding constant of the order $9.04 \times 10^4 \text{ M}^{-2}$ for NaOAc and $1.55 \times 10^2 \text{ M}^{-1}$ for Cu^{2+} ion. Selectivity of **L1** for Cu^{2+} ion and **L2** for AcO^- ions with spectroscopic detection

limit of 1.81 and 0.61 ppm, respectively, implies the practical utility of receptors. The receptors **L1**, **L2** and **L3** prove their efficacy in the detection of AcO^- and Cu^{2+} ions signifying their role as dual sensor. Binding studies performed with $\text{Cu}(\text{OAc})_2$ reflects the utility of receptor **L1** as 'OR' gate, **L2** and **L3** as 'INHIBIT' molecular logic gates.

Acknowledgements

Authors express their gratitude to the Director and the HOD (Department of Chemistry) NITK Surathkal for the providing the research infrastructure. DRT thanks DST (SB/FT/CS-137/2012) for the financial support of this work. SP is thankful to NITK for the Research fellowship. We thank IITM, Chennai and MIT Manipal for the mass and NMR analysis.

Disclosure statement

No potential conflict of interest was reported by the authors.

Funding

This work was supported by Science and Engineering Research Board [SB/FT/CS-137/2012].

Supplemental Material

The underlying research materials for this articles can be accessed at <http://dx.doi.org/10.1080/10610278.2017.1298764>.

References

- (1) Suganya, S.; Zo, H.J.; Park, J.S.; Velmathi, S. *Ind. Eng. Chem. Res.* **2014**, *53*, 9561–9569.
- (2) Schneider, H.J.; Yatsimirsky A.K. *Chem. Soc. Rev.* **2008**, *37*, 263–277.
- (3) (a) Schmidtchen, F.P.; Berger, M. *Chem. Rev.* **1997**, *97*, 1609–1646; (b) Mànez, R.M.; Sacenón, F. *Chem. Rev.* **2003**, *103*, 4419–4476; (c) Gunnlaugsson, T.; Glynn, M.; Tocci, G.M.; Kruger, P.E.; Pfeiffer, F.M. *Coord. Chem. Rev.* **2006**, *250*, 3094–3117; (d) Saksai, C.; Tuntulani, T. *Chem. Soc. Rev.* **2003**, *32*, 192–202; (e) Gunnlaugsson, T.; Davis, A.P.; O'Brien, J.E.; Glynn, M. *Org. Lett.* **2002**, *4*, 2449–2452.
- (4) Kumari, N.; Dey, N.; Bhattacharya, S. *RSC Adv.* **2014**, *4*, 4230–4238.
- (5) Patil, S.R.; Nandre, J.P.; Jadhav, D.; Bothra, S.; Sahoo, S.K.; Devi, M.; Pradeep, C.P.; Mahulikar, P.P.; Patil, U.D. *Dalton Trans.* **2014**, *43*, 13299–13306.
- (6) Deraeve, C.; Boldron, C.; Maraval, A.; Mazarguil, H.; Gornitzka, H.; Vendier, L.; Pitié, M.; Meunier, B.; *Chem.–Eur. J.* **2008**, *14*, 682–696.
- (7) Sha, J.; Tong, C.; Zhang, H.; Feng, L.; Liu, B.; Lü, C. *Dyes Pigm.* **2015**, *113*, 102–109.
- (8) Yang, L.; Song, Q.; Damit-Og, K.; Cao, H. *Sens. Actuators B* **2013**, *176* (181), 185.
- (9) He, X.; Zhang, J.; Liu, X.; Dong, L.; Li, D.; Qiu, H.; Yin, S. *Sensor Actuat B-Chem* **2014**, *192*, 29.
- (10) Hsieh, Y.C.; Chir, J.L.; Wu, H.H.; Chang, P.S.; Wu, A.T. *Carbohydr. Res* **2009**, *344*, 2236.
- (11) Wang, X.; Zhao, J.; Guo, C.; Pei, M.; Zhang, G. *Sensor Actuat B-Chem* **2014**, *193*, 157.
- (12) Ye, H.; Ge, F.; Chen, X.C.; Li, Y.; Zhang, H.; Zhao, B.X.; Miao, J.Y. *Sensor Actuat B-Chem* **2013**, *182*, 273.
- (13) Huang, J.; Ma, X.; Liu, B.; Cai, L.; Li, Q.; Zhang, Y.; Jiang, K.; Yin, S. *J. Lumin* **2013**, *141*, 130.
- (14) Yin, S.; Leen, V.; Snick, S.V.; Boens, N.; Dehaen, W. *Chem. Commun* **2010**, *46*, 6329–6331.
- (15) (a) Custelcean, R.; Moyer, B.A.; Hay, B.P. *Chem. Commun.* **2005**, 5971; (b) Hay, B.P.; Firman, T.K.; Moyer, B.A. *J. Am. Chem. Soc.* **2005**, *127*, 1810, 127.
- (16) Busschaert, N.; Wenzel, M.; Light, M.E.; Iglesias-Hernández, P.; Pérez-Tomás, R.; Gale, P.A. *J. Am. Chem. Soc.* **2011**, *133*, 14136.
- (17) Custelcean, R.; Bosano, J.; Bonnesen, P.V.; Kertesz, V.; Hay, B.P. *Angew. Chem., Int. Ed.* **2009**, *48*, 4025.
- (18) Ravikumar, I.; Lakshminarayanan, P.S.; Arunachalam, M.; Suresh, E.; Ghosh, P. *Dalton Trans.* **2009**, 4160.
- (19) Dey, S.K.; Das, G. *Dalton Trans.* **2011**, *40*, 12048.
- (20) dos Santos, C.M.G.; Boyle, E.M.; De Solis, S.; Kruger, P.E.; Gunnlaugsson, T. *Chem. Commun.* **2011**, 12176.
- (21) Stanley, C.E.; Clarke, N.; Anderson, K.M.; Elder, J.A.; Lenthall, J.T.; Steed, J.W. *Chem. Commun.* **2006**, 3199.
- (22) Basaran, I.; Wang, X.; Alamgir, A.; Wang, J.; Haque, S.A.; Zhang, Y.; Powell, D.R.; Leszczynski, J.; Hossain, MdA. *Tetrahedron Lett.* **2015**, *56*, 657–661.
- (23) Sharma, D.; Mistry, A.R.; Bera, R.K.; Sahoo, S.K. *Supramol. Chem.* **2013**, *25* (4), 212–220.
- (24) Sharma, D.; Bera, R.K.; Sahoo, S.K. *Spectrochim. Acta Part A: Mol. Biomol. Spectrosc.* **2013**, *105*, 477–482.
- (25) Sharma, D.; Moirangthem, A.; Roy, S.M.; Kumar, A.S.K.; Nandre, J.P.; Patil, U.D.; *J. Photochem. Photobio. B* **2015**, *148*, 37–42.
- (26) Raymo, F.M. *Adv. Mater.* **2002**, *14*, 401–414.
- (27) Balzani, V.; Credi, A.; Venturi, M. *ChemPhysChem* **2003**, *4*, 49–59.
- (28) Callan, J.F.; de Silva, A.P.; Magri, D.C. *Tetrahedron.* **2005**, *61*, 8551–8588.
- (29) Saghatelian, A.; Völcker, N.H.; Guckian, K.M.; Lin, V.S.-Y.; Ghadiri, M.R. *J. Am. Chem. Soc.* **2003**, *125*, 346–347.
- (30) Lin, J.-H.; Tseng, W.-L. *Analyst.* **2014**, *139*, 1436–1441.
- (31) Margulies, D.; Melman, G.; Shanzer, A. *J. Am. Chem. Soc.* **2006**, *128*, 4865–4871.
- (32) Gabr, A.A. *Spectrochim. Acta A* **1990**, *46*, 1751–1757.
- (33) Thiampanya, P.; Muangsinsin, N.; Pulpoka, B. *Org. Lett.* **2012**, *14* (16), 4050–4053.
- (34) Yadav, U.N.; Pant, P.; Sahoo, S.K.; Shankarling, G.S. *RSC Adv.* **2014**, *4*, 42647–42653.
- (35) Benesi, H.; Hildebrand, H. *J. Am. Chem. Soc.* **1948**, *71*, 2703–2707.
- (36) Suganya, S.; Zob, H.J.; Park, J.S.; Velmathi, S. *J. Mol. Recognit.* **2014**, *27*, 689–695.
- (37) Udhayakumari, D.; Saravanamoorthy, S.; Velmathi, S. *Materials Science and Engineering: C* **2012**, *32* (7), 1878–1882.
- (38) Shellaiyah, M.; Wu, Y.-H.; Singh, A.; Ramakrishnam Raju, M.V.; Lin, H.-C. *J. Mater. Chem. A*, **2013**, *1*, 1310–1318.
- (39) Sharma, D.; Ashok Kumar, S.K.; Sahoo, S. K. *Tetrahedron Letts* **2014**, *55*, 927–930.
- (40) Farinha, A.S.F.; Tomé, A.C.; Cavaleiro, J.A.S. *Tetrahedron* **2010**, *66*, 7595–7599.

- (41) Boiocchi, M.; Del Boca, L.; Gómez, D.E.; Fabbrizzi, L.; Licchelli, M.; Monzani, E. *J. Am. Chem. Soc.* **2004**, *126*, 16507–16514.
- (42) Makal, A.; Schilf, W.; Bohdan Kamieński, B.; Anna Szady-Chelmieniecka, A.; Eugeniusz Grech, E.; Woźniak, K. *Dalton Trans.* **2011**, *40*, 421.
- (43) (a) Kuwar, A.; Patil, R.; Singh, A.; Sahoo, S.K.; Marek, J.; Singh, N. *J. Mater. Chem. C* **2015**, *3*, 453–460. (b) Margulies, D.; Felder, C.E.; Melman, G.; Shanzer, A. *J. Am. Chem. Soc.* **2007**, *129*, 347–354.
- (44) Magri, D.C.; Brown, G.J.; McClean, G.D.; de Silva, A.P. *J. Am. Chem. Soc.* **2006**, *128*, 4950–4951.
- (45) (a) Kaur, N.; Alreja, P. *Tetrahedron Lett.* **2015**, *56*, 182–186; (b) Szacilowski, K.; Infochemistry. Wiley: Chichester, **2012**; (c) de Silva, A.P. Royal Society of Chemistry. Cambridge, **2013**; (d) de Silva, A.P.; McClenaghan, N.D. *Chem.–Eur. J.* **2002**, *8*, 4935–4945; (e) Rurack, K.; Trieflinger, C.; Koval'chuck, J.; Daub, J. *J. Chem. Eur. J.* **2007**, *13*, 8998–9003.
- (46) Wang, L.; Li, B.; Zhang, L.; Luo, Y. *Dalton Trans.* **2013**, *42*, 459–465.